

Prediction of lymph node metastasis in rectal cancer: comparison between shear-wave elastography based ultrasonics and MRI

Meng-Fei Xian* 

Xin Zheng* 

Jian-Bo Xu 

Xin Li 

Li-Da Chen 

Wei Wang 

PURPOSE

We aimed to explore the diagnostic efficiency of shear-wave elastography (SWE) ultrasonics in the preoperative prediction of lymph node (LN) metastasis in rectal cancer.

METHODS

This study included 87 patients with pathologically confirmed rectal cancer, with data gathered from August 2017 to August 2018. A total of 1044 ultrasonics features of rectal tumor were collected with AK software from the SWE examinations. The least absolute shrinkage and selection operator (LASSO) regression model was used for feature selection and building a SWE ultrasonics signature. The diagnostic performance was evaluated with an area under the receiver operating characteristic curve (AUC) analysis. Then, the diagnostic performance of the SWE ultrasonics signature was compared with magnetic resonance imaging (MRI).

RESULTS

Of the 87 patients, 40 (46.0%) had LN metastasis. Thirteen ultrasonics features of rectal tumor were selected as the most significant features. The SWE ultrasonics signature correlated with LN metastasis ($p < 0.001$). Patients with LN metastasis had higher signature than patients without LN metastasis. In terms of diagnostic performance, SWE ultrasonics signature was significantly superior to MRI (AUC, 0.883 vs. 0.760, $p = 0.034$). The diagnostic accuracy, sensitivity, specificity, positive predictive value (PPV), and negative predictive value (NPV) of SWE ultrasonics signature were 82.8%, 87.5%, 78.8%, 77.8%, and 88.1%, respectively, while those of MRI were 75.9%, 77.5%, 74.5%, 72.1%, and 79.6%, respectively.

CONCLUSION

SWE ultrasonics is a more accurate predictive method for identifying LN metastasis preoperatively than MRI. Thus, SWE ultrasonics might be used to better guide preoperative individual therapies for patients with rectal cancer.

From the Department of Medical Ultrasonics (M.F.X.), East division of the First Affiliated Hospital of Sun Yat-sen University, Guangzhou, China; Department of Medical Ultrasonics (X.Z., L.D.C. ✉ chenlda@mail.sysu.edu.cn, W.W. ✉ wangw73@mail.sysu.edu.cn), Ultrasonics Artificial Intelligence X-Lab, Institute of Diagnostic and Interventional Ultrasound, The First Affiliated Hospital of Sun Yat-Sen University, Guangzhou, China; Department of Gastrointestinal Surgery (J.B.X.), The First Affiliated Hospital of Sun Yat-Sen University, Guangzhou, China; Research Center of GE Healthcare (X.L.), Shanghai, China.

*Meng-Fei Xian and Xin Zheng contributed equally to this work.

Received 7 February 2020; revision requested 23 March 2020; last revision received 27 May 2020; accepted 2 June 2020.

Published online 19 April 2021.

DOI 10.5152/dir.2021.20031

Colorectal cancer is the third most common cancer and the fourth frequent cause of cancer death worldwide; approximately one-third of these tumors is rectal cancer (1). Accurate identification of lymph node (LN) involvement is important in determining whether rectal cancer patients require preoperative neoadjuvant therapy (2, 3). Therefore, accurate prediction of LN metastasis can provide valuable information and is crucial for treatment decisions and prognosis (4).

According to ESGAR guidelines (European Society of Gastrointestinal and Abdominal Radiology) 2016 recommendations, magnetic resonance imaging (MRI) is considered the gold standard for rectal cancer staging (3, 5–7). However, MRI is not perfect for determination of LNs status, and the criteria used to indicate LN metastasis may vary in different institutions (8). A meta-analysis found MRI to be 77% sensitive (95% CI, 69%–84%) and 71% specific (95% CI, 59%–81%) for detection of LN involvement (9). In addition, endoscopic ultrasonography (EUS) is also a widely used method for patients with rectal cancer, but the accuracy of EUS to identify LN involvement is inferior to that of both computed tomography (CT) and MRI because of a lack of visualization of the entire mesorectum and the difficulty in accurately distinguishing benign from malignant nodes based only on the shape, echo fea-

You may cite this article as: Xian MF, Zheng X, Xu JB, Li X, Chen LD, Wang W. Prediction of lymph node metastasis in rectal cancer: comparison between shear-wave elastography and MRI. *Diagn Interv Radiol* 2021; 27:424–431

ture and size criterion (10–13). Given these limitations, neither MRI nor EUS is an ideal method for diagnosing LN status in rectal cancer.

Radiomics, extracted from CT, MRI, or positron emission tomography images, uses a set of quantitative features to describe the geometrical structure, intensity distribution and texture of a region of interest (ROI). These features include shape, edge, and texture metrics, which can provide important insights into the tumor phenotype and the interaction of the tumor with its microenvironment (14, 15). Similarly, we have applied the concept to computing quantitative ultrasound imaging, a term defined as “ultrasomics” (16). Shear-wave elastography (SWE), an ultrasound elastography technique that provides a real-time two-dimensional (2D) quantifiable image of tissue stiffness (17), has emerged as an efficient tool in detection of malignancies. The report of Wang et al. (18) confirmed that the deep learning of elastography showed a better prediction of liver fibrosis staging compared with transient elastography, 2D-SWE, and serological examinations. Therefore, SWE-based ultrasomics has a promising future in staging and prediction.

To our knowledge, there has been no study that combines SWE and ultrasomics to predict the LN metastasis. In order to build a robust model, we hypothesized that SWE ultrasomics could be a better option in LN status prediction of colorectal cancer patients. Therefore, the purpose of this study was to evaluate the accuracy of LN metastasis identification before surgical resection using SWE ultrasomics of primary tumor and compare it with MRI.

Methods

Patients

This prospective, single-center study (clinical trial ChiCTR-DDD-16008940) was

approved by the Institutional Review Board of our hospital, and has obtained the informed consent from all individual participants included in the study. From August 2017 to August 2018, we enrolled consecutive patients with rectal cancer in our institution. In total, 87 patients with rectal cancer were eventually included in the study according to the inclusion and exclusion criteria. Patients meeting the following criteria were included: a) tumor located less than 15 cm from the anal verge, within the scan feasibility; b) patients deemed operable based on the determination of a multidisciplinary team discussion, and surgical resection performed within 2 weeks after EUS and MRI examinations; c) LNs dissected intraoperatively with patho-

logical confirmation; d) tumor confirmed as rectal adenocarcinoma on histopathology; and e) SWE and MRI both examined. Exclusion criteria were as follows: a) history of chemotherapy or surgical treatment for rectal tumor; b) no pathological assessment of LN metastasis; or c) no MRI. Fig. 1 shows the flowchart. Clinical and laboratory parameters of the study population were recorded.

SWE image acquisition

The EUS and SWE image acquisitions were obtained by a radiologist with at least 5 years of experience in ultrasound examinations and 3 years of experience in SWE scans. The radiologist knew that the patients had rectal lesions but was

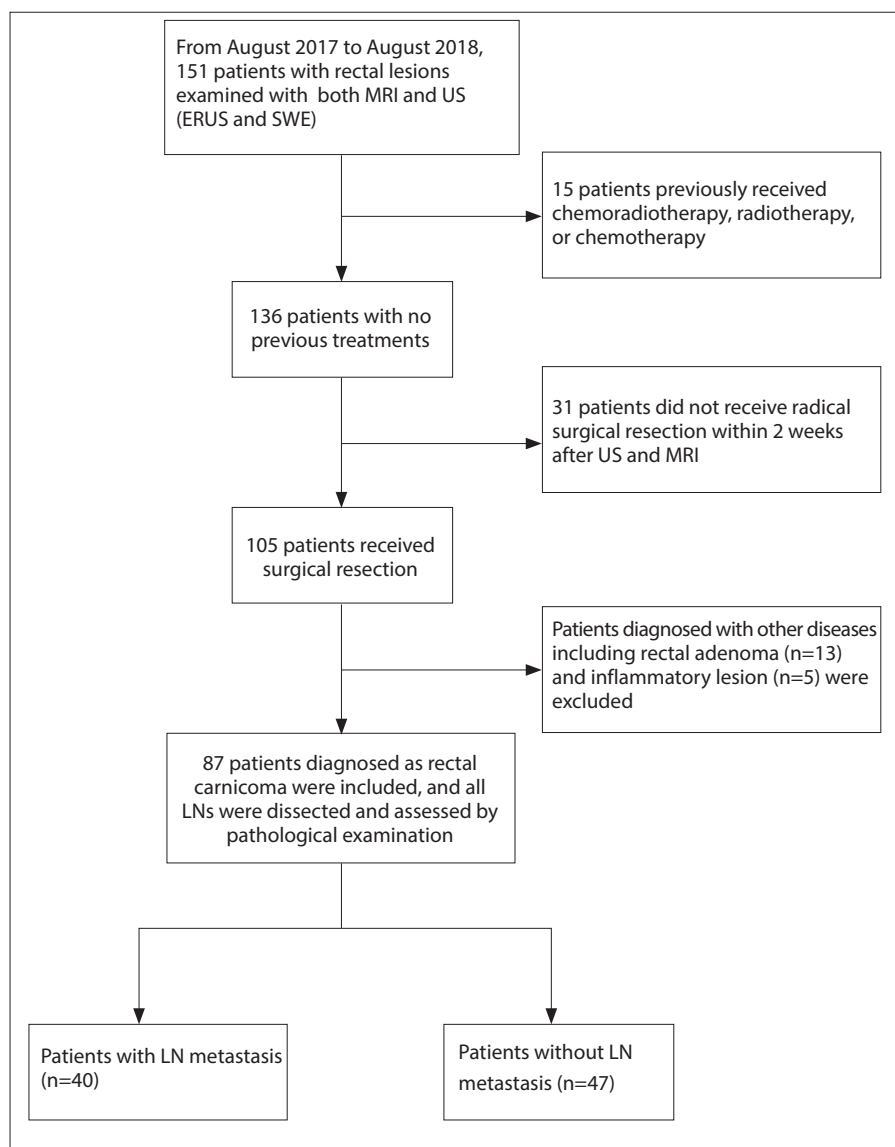


Figure 1. The flowchart of patient selection. MRI, magnetic resonance imaging; US, ultrasonography; ERUS, endorectal ultrasonography; SWE, shear-wave elastography; LN, lymph node.

Main points

- Ultrasomics based on shear-wave elastography was used for preoperative prediction of LN metastasis in patients with rectal cancer.
- Patients with LN metastasis had higher signature than patients without LN metastasis.
- SWE ultrasomics showed superior diagnostic performance compared with MRI for identifying the LN status.
- Ultrasomics can guide preoperative adjuvant chemoradiation of rectal cancer patients.

blinded to the results of the biopsy and any imaging or endoscopy results. Sodium phosphate was used to give an enema to all patients without sedation, 2 hours prior to the inspection. The EUS and SWE images were acquired by using an SE12-3 intra-luminal transrectal high-frequency (8 MHz) probe (SuperSonic Imagine) and the Aixplorer US diagnostic imaging system (SuperSonic Imagine). Before the insertion of the probe, 200–500 mL of 0.9% NaCl was injected into the rectum to fully distend. The settings were adjusted to specified parameters at each examination, including the gain, depth, focus, and time gain compensation. After EUS scanning, the supersonic shear-wave image was superimposed on the B-mode image to obtain a fan-shaped region-of-interest, indicating the beginning of SWE acquisition. Tissue stiffness in the region of interest was represented by a color map ranging from blue (soft tissue) to red (hard tissue). Settings were adjusted to penetration, with the maximum elasticity scale at 90–100 kPa. The transducer was placed close to the tumor without pressure, and the image was frozen when signal of the color map was stabilized.

Acquisition of SWE ultrasonics features

The image that displayed the deepest section of tumor infiltration into the rectal wall was selected to place the color map of the SWE. The SWE ultrasonics features of rectal tumor were extracted using AK software (Artificial Intelligence Kit, version X, GE Healthcare). The AK software is an artificial intelligence software for extracting ultrasonics or radiomics features. After importing one SWE image into AK software, the radiologist who was unaware of the final diagnosis, delineated a circular ROI covering the rectal tumor, and ran the program of the software. Then, the software automatically extracted the SWE ultrasonics features from the ROI of the rectal tumor on the SWE image.

A total of 1044 features were finally extracted from each single image of each patient. All features were grouped under the following categories: histogram parameters, grey level co-occurrence matrix (GLCM) parameters, grey level run-length matrix (GLRLM) parameters and texture parameters, which can reflect the main features of the focus of medical images comprehensively.

Intraobserver and interobserver reproducibility of feature extraction

For testing the intraobserver reproducibility, ROIs of 30 patients randomly selected from the training set were delineated by the radiologist no. 1 with at least 5 years of experience who performed the SWE ultrasonics extraction 1 month later. Moreover, to assess the inter-observer reproducibility of SWE ultrasonics feature extraction, ROIs of another 30 patients randomly selected from the training set were delineated by two radiologists (no. 1 and no. 2 with over 5 years of experience) one month later.

MRI examination

The rectal MRI examination was performed using a 3T MRI scanner (Magnetom Verio; Siemens Healthcare) equipped with an 8-channel body-matrix coil. All patients were routinely injected intramuscularly with 20 mg of anisodamine to minimize intestinal peristaltic movement. In order to display the boundary of the tumor more clearly, 30–120 mL of ultrasound gel was injected into the rectum before the initial MRI scan. Gadolinium (gadopentetate dimeglumine, Kangcheng) was injected intravenously using a power injector (Medrad) at 0.2 mmol/kg of body-weight at a rate of 3.0 mL/s. Conventional rectal MRI included axial, sagittal and coronal T2-weighted turbo spin-echo (T2-TSE). It also included T1-TSE and T2-TSE perpendicular to the long axis of the rectum covering the whole tumor. A prototype diffusion-weighted imaging (DWI) sequence was performed prior to gadolinium injection to acquire the intravoxel incoherent motion data. A total of 14 b values (0, 5, 10, 20, 30, 40, 60, 80, 100, 150, 200, 400, 600, and 1000 s/mm²) were applied using a single-shot spin-echo echo-planar-imaging sequence.

An abdominal MRI radiologist with more than ten years of experience reassessed the following features of the LNs: shape, signal heterogeneity, and diameter of the largest LN on T2-weighted imaging, whether a high-signal-intensity LN was detected on DWI, and whether there was an enhancement pattern in the arterial phase. Finally, the malignancy of the LNs was estimated. LNs on high-resolution MRI meeting any of the following criteria were diagnosed as metastasis: a) node with an irregular shape and a heterogeneous signal on T2-weighted imaging, b) node with high signal intensity on DWI, and c) node with a high percent enhancement in the arterial phase (5, 19–21).

Histopathological examination

All the enrolled patients underwent surgical resection of the tumor within 2 weeks after EUS, SWE, and MRI examinations. The tissue sections were assessed by a pathologist with more than 10 years of experience in gastroenterological diseases who was blinded to any imaging or endoscopy results. Referring to the guidelines of the American Joint Committee on Cancer, the pathologist determined the depth of tumor infiltration and LN metastasis (22).

Statistical analysis

Statistical analyses were performed by using R version 3.3.3. (<http://www.r-project.org/>) and MedCalc (10.4.7.0). All statistical tests were two-sided, and *p* values of less than 0.05 were considered statistically significant.

Categorical variables were compared with the chi-square test. Continuous variables were compared with *t* test. Least absolute shrinkage and selection operator (LASSO) was used for data dimension reduction, feature selection, and ultrasonics signature building. This method minimized the residual sum of squares, subject to the sum of the absolute value of the coefficients being less than a tuning parameter. As the tuning parameter gets smaller, this may cause some coefficients to be shrunk towards zero or set to be zero. LASSO was first used to select the most useful predictive features from all features. Then, a regression equation was established based on the regression coefficients and parameters of LASSO. A ultrasonics signature was calculated for each patient via the regression equation. A receiver operating characteristic curve (ROC) analysis was performed, and the area under the receiver operating characteristic curve (AUC) analysis was used to evaluate the diagnostic performance. An optimal cutoff value that maximized the sum of the sensitivity and specificity was used to calculate sensitivity, specificity, positive predictive value (PPV), and negative predictive value (NPV). In addition, the comparison between AUC curves was made by the DeLong test using Medcalc statistical software, which was used to compare the difference in diagnostic performance between SWE ultrasonics and MRI.

The reproducibility of the intra- and interobserver was assessed by the intraclass correlation coefficient (ICC). An ICC ≥ 0.75 suggested high consistency, 0.50–0.74 suggested moder-

Table 1. Basic characteristics of patients			
Characteristics	LN metastasis (+)	LN metastasis (-)	<i>p</i>
Number of patients, n (%)	40 (46.0)	47 (54.0)	
Gender, n (%)			0.507
Male	21 (52.5)	28 (59.6)	
Female	19 (47.5)	19 (40.4)	
Age (years), mean±SD (range)	58±13 (29–77)	61±10 (38–78)	0.196
Histologic T stage, n (%)			0.000*
T1/2	1 (2.5)	22 (46.8)	
T3/4	39 (97.5)	25 (53.2)	
Size			0.189
<3 cm	7 (17.5)	16 (34.1)	
3–6 cm	31 (77.5)	30 (63.8)	
>6 cm	2 (5.0)	1 (2.1)	
Location, n (%)			0.124
Upper	17 (42.5)	13 (27.6)	
Middle	14 (35.0)	14 (29.8)	
Lower	9 (22.5)	20 (42.6)	
CEA, n (%)			0.138
Normal (< 5 µg/L)	21 (52.5)	32 (68.0)	
Abnormal (> 5 µg/L)	19 (47.5)	15 (32.0)	
CA19-9 level, (%)			0.209
Normal (<35 U/mL)	38 (95.0)	47 (100)	
Abnormal (>35 U/mL)	2 (5.0)	0 (0)	
Hemoglobin in stool, n (%)			0.775
Normal	5 (12.5)	6 (12.8)	
Abnormal	35 (87.5)	41 (87.2)	
Transferrin in stool, n (%)			0.702
Normal	8 (20.0)	11 (23.4)	
Abnormal	32 (80.0)	36 (76.6)	
White blood cells in stool, n (%)			0.989
Normal	34 (85.0)	40 (85.1)	
Abnormal	6 (15.0)	7 (14.9)	
Red blood cells in stool, n (%)			0.360
Normal	32 (80.0)	41 (87.2)	
Abnormal	8 (20.0)	6 (12.8)	

The *p* value is derived from the comparison between the LN metastasis (+) and the LN metastasis (-), using the student's *t*-test for age or chi-square test for other clinicopathologic variables.
LN, lymph node; SD, standard deviation; CEA, carcinoembryonic antigen; CA19-9, cancer antigen 19-9.
**p* < 0.05.

ate consistency, and <0.50 suggested low consistency. The *p* values of less than 0.05 indicate differences between ICC and zero.

Results

All 87 patients (male 49, female 38) were confirmed by pathology, including 40

(46.0%) with LN metastasis and 47 (54.0%) without LN metastasis (Table 1). The average age of the patients with LN metastasis was 58 years (range, 29–77 years), including 21 males (52.5%) and 19 females (47.5%). The average age of the patients without LN metastasis was 60 years (range, 38–78 years), including 28 males (59.5%) and 19 females

(40.4%). There were no significant differences between patients with and without LN metastasis in terms of gender, age, tumor size, tumor location, serological examination (CEA and CA19-9 level), fecal occult blood test (hemoglobin in the stool, transferrin in the stool) and stool routine tests (white blood cells and red blood cells in the stool) (all *p* > 0.05). Of the patients with LN metastasis, only one patient was T1/2, and 39 patients were T3/4 (Fig. 2). Of the patients without LN metastasis, 22 patients were T1/2, and 25 patients were T3/4 (Fig. 3). A significant difference of T stage between the two groups of patients (*p* < 0.001) was found. LN metastasis was more common in T3/4 patients than in T1/2 patients.

The intraobserver reproducibility of the SWE ultrasomics features extracted from the ROI was high, with ICCs ranging from 0.717 (*p* = 0.235) to 0.986 (*p* = 0.000). The interobserver reproducibility of the features extracted from the ROI was also moderate to high, with ICCs ranging from 0.663 (*p* = 0.548) to 0.958 (*p* = 0.000). The features with low reproducibility that had intra- or interobserver ICC of <0.75 were excluded.

On the basis of the LASSO regression model, 1044 features of each patient were reduced to 13 selected predictors (Table 2). Among them, 2 features in histogram parameters, 2 features in GLCM parameters, 1 feature in GLCM parameters and 8 features in GLRLM parameters were extracted. Then, the calculation of SWE ultrasomics signature for each patient was performed using the following constructed formula based on the LASSO regression coefficients and 13 selected predictors:

$$\begin{aligned} \text{SWE ultrasomics signature} = & 4.980560 \\ & + 0.000002 \times \text{RelativeDeviation} - 0.003763 \\ & \times \text{Percentile90} + 23.82352 \times \text{InverseDifferenceMoment_AllDirection_offset3_SD} \\ & - 0.525355 \times \text{GLCMEntropy_angle45_offset5} - 0.001977 \times \text{Inertia_AllDirection_offset7_SD} \\ & - 0.003099 \times \text{ShortRunHighGreyLevelEmphasis_AllDirection_offset1_SD} \\ & + 0.013506 \times \text{RunLengthNonuniformity_AllDirection_offset3_SD} \\ & + 1571.633 \times \text{ShortRunLowGreyLevelEmphasis_AllDirection_offset5_SD} \\ & + 497.2829 \times \text{LongRunLowGreyLevelEmphasis_AllDirection_offset5_SD} \\ & + 837.4631 \times \text{ShortRunLowGreyLevelEmphasis_AllDirection_offset7_SD} \\ & + 473.2587 \times \text{ShortRunLowGreyLevelEmphasis_AllDirection_offset8_SD} \\ & + 21.41898 \times \text{ShortRunLowGreyLevelEmphasis_AllDirection_offset9_SD} \\ & - 0.000003 \times \text{HighIntensityLargeAreaEmphasis} \end{aligned}$$

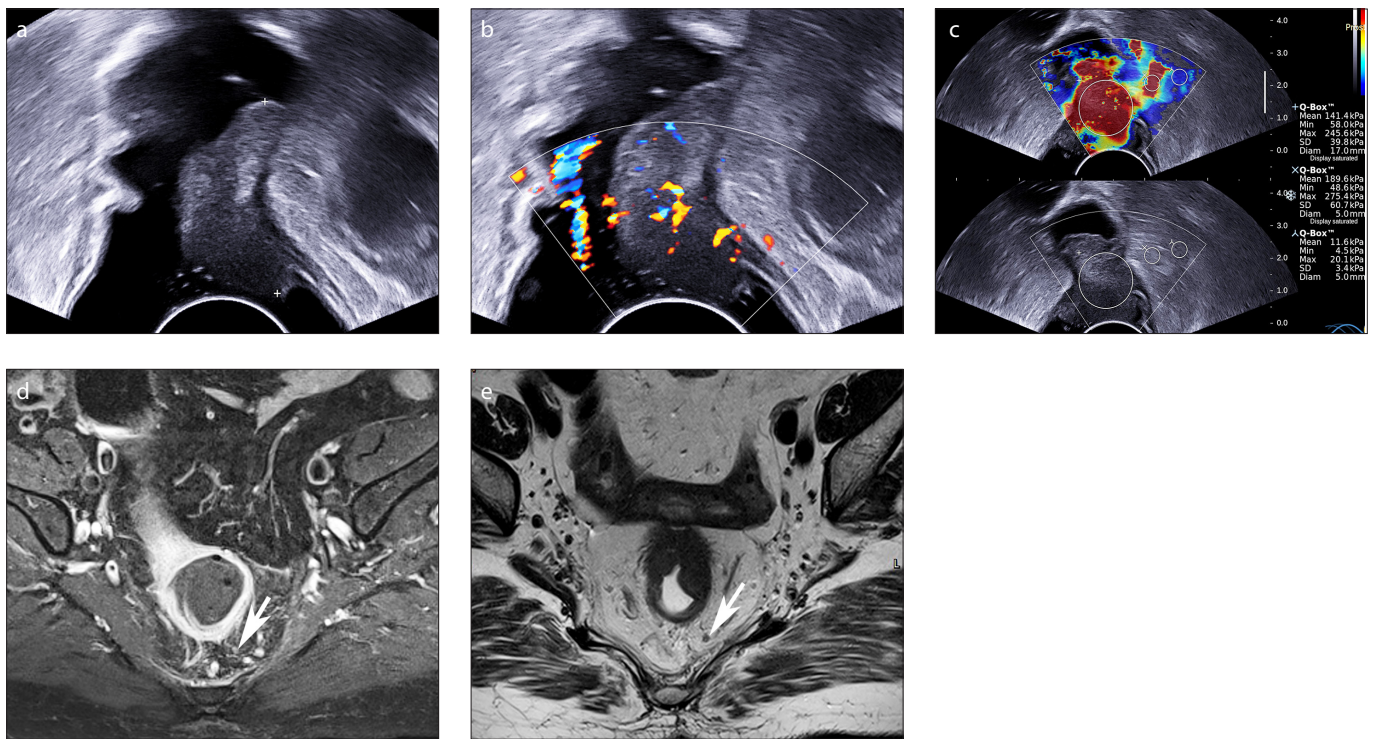


Figure 2. a–e. EUS, SWE, and MRI images of a 67-year-old female patient with rectal cancer. The postoperative pathological stage was T3N1M0. The SWE ultrasonomics signature of the patient was higher than cutoff value (-0.10691 vs. -0.1171), which can be diagnosed as LN metastasis (+), while the MRI diagnosis was LN metastasis (-). B-mode ultrasound image (a) of rectal adenocarcinoma shows the diameter of the lesion. Image (b) shows color Doppler sonography of rectal adenocarcinoma. The top panel in (c) shows the SWE image, the biggest circle ROI was placed in the rectal tumor for the extraction of SWE ultrasonomics features; the bottom panel is the corresponding B-mode ultrasound image. Contrast-enhanced T1-weighted MRI image (d) shows regularly shaped LNs (white arrow). T2-weighted MRI image (e) shows the LN as regularly shaped, with well-defined contours, and homogeneous signal (white arrow).

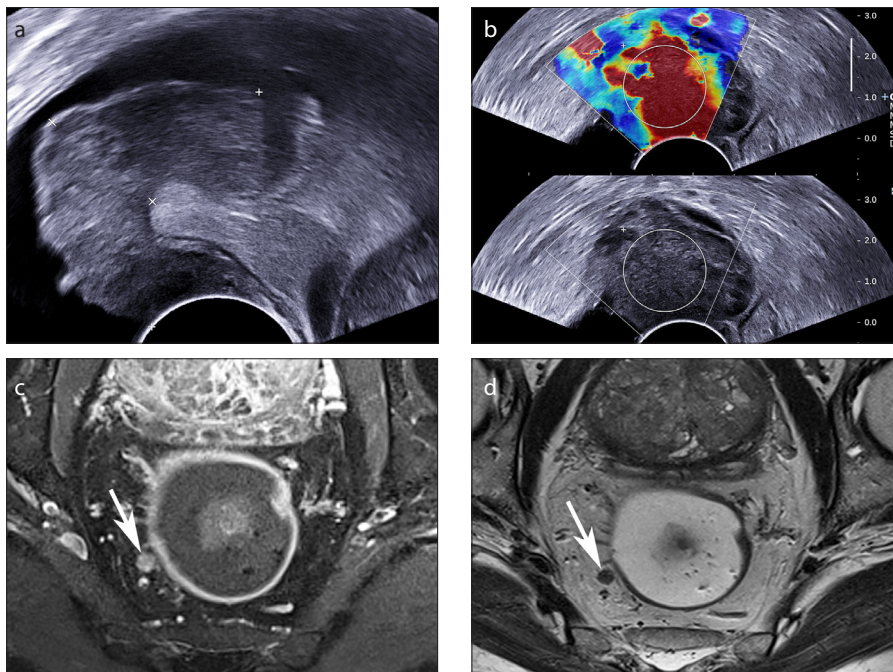


Figure 3. a–d. EUS, SWE, and MRI images of a 78-year-old male patient with rectal cancer. The postoperative pathological stage was T3N0M0. The SWE ultrasonomics signature of the patient was lower than cutoff value (-1.27343 vs. -0.1171), which can be diagnosed as LN metastasis (-), while the MRI diagnosis was LN metastasis (+). B-mode ultrasound image (a) shows the rectal adenocarcinoma, with the range of the tumor marked. The top panel in (b) shows the SWE image, with the circle ROI was placed in the rectal tumor for the extraction of SWE ultrasonomics features; bottom panel is the corresponding B-mode ultrasound image. Contrast-enhanced T1-weighted image (c) shows irregularly shaped LN (white arrow). T2-weighted image (d) reveals the LN irregularly shaped with heterogeneous signal (white arrow).

The SWE ultrasonomics signature correlated with LN metastasis for patients with rectal cancer ($p < 0.001$). Patients with LN metastasis had higher signature than did patients without LN metastasis (Fig. 4). The average score of a positive LN was 0.313 ± 0.498 (-0.567, 1.884), while that of a negative LN was -0.634 ± 0.719 (-2.848, 0.774).

Of the 47 patients without LN metastasis, 37 (78.7%) were diagnosed accurately by SWE ultrasonomics and 35 (74.5%) by MRI. Of the 40 patients with LN metastasis, 35 (87.5%) were identified accurately by SWE ultrasonomics, while only 31 (77.5%) were identified by MRI. Fifteen (17.2%) patients and 21 (24.1%) patients were misdiagnosed by SWE ultrasonomics and MRI, respectively (Table 3).

On MRI, 43 patients were diagnosed with LN metastasis. All of these patients had LNs greater than 5 mm in diameter. There were 23 patients with LNs with irregular shapes, and 43 patients had ill-defined borders and heterogeneous signals on T2-weighted imaging (Fig. 3). Furthermore, 37 patients had nodes with high signal intensity on DWI, and 33 patients had LNs with a higher percent enhancement in the arterial phase.

Table 2. The 13 predictors selected from the 1044 SWE ultrasonics features

Parameters	Selected features	Coefficients
Histogram parameters	RelativeDeviation	0.000002
	Percentile90	0.003763
GLCM parameters	InverseDifferenceMoment_AllDirection_offset3_SD	23.82352
	GLCMEntropy_angle45_offset5	0.525355
Texture parameter	Inertia_AllDirection_offset7_SD	0.001977
GLRLM parameters	ShortRunHighGreyLevelEmphasis_AllDirection_offset1_SD	0.003099
	RunLengthNonuniformity_AllDirection_offset3_SD	0.013506
	ShortRunLowGreyLevelEmphasis_AllDirection_offset5_SD	1571.633
	ShortRunLowGreyLevelEmphasis_AllDirection_offset7_SD	497.2829
	ShortRunLowGreyLevelEmphasis_AllDirection_offset8_SD	837.4631
	ShortRunLowGreyLevelEmphasis_AllDirection_offset9_SD	473.2587
	LongRunLowGreyLevelEmphasis_AllDirection_offset5_SD	21.41898
	HighIntensityLargeAreaEmphasis	0.000003

There were four kinds of SWE ultrasonics parameters listed in column 1 which were extracted by AK software in our study, and the four parameters contain 13 selected predictors in column 2. The coefficients of regression model are listed in column 3.

Table 3. The diagnostic results of SWE ultrasonics and MRI

	Pathology		Total
	LN metastasis (+), n=40	LN metastasis (-), n=47	
SWE ultrasonics, n (%)			
LN metastasis (+)	35 (87.5)	10 (21.3)	45
LN metastasis (-)	5 (12.5)	37 (78.7)	42
MRI, n (%)			
LN metastasis (+)	31 (77.5)	12 (25.5)	43
LN metastasis (-)	9 (22.5)	35 (74.5)	44

Variables represent the number and percentage of cases diagnosed by SWE/MRI or pathology. SWE, shear-wave elastography; MRI, magnetic resonance imaging; LN, lymph node.

Among the 21 patients misdiagnosed by MRI, 17 patients were misdiagnosed by MRI but correctly diagnosed by SWE ultrasonics. Among the 17 patients misdiagnosed by MRI, 9 patients had LN metastasis on pathology, one appeared to have a regular shape (Fig. 2), 3 appeared to have well-defined contours, and 5 appeared to have homogeneous signal on T2-weighted imaging. In the group of 8 patients with no LN metastasis on pathology that were misdiagnosed by MRI, 2 appeared to have ill-defined LN borders, 3 appeared to have heterogeneous signals, one appeared to have an irregularly shaped LN with heterogeneous signal (Fig. 3), and one appeared to have an irregularly shaped LN, with ill-defined border and heterogeneous signal on T2-weighted imaging. Another patient appeared to have a high signal intensity LN on DWI.

For the discrimination of LN metastasis, the diagnostic performance of SWE ultrasonics signature was significantly higher than that of MRI (AUC, 0.883 vs. 0.760, $p = 0.034$) (Fig. 5). The diagnostic accuracy, sensitivity, specificity, PPV and NPV of SWE ultrasonics signature were 82.8%, 87.5%, 78.8%, 77.8%, and 88.1%, respectively, which are higher than those of MRI. The accuracy, sensitivity, specificity, PPV, and NPV of MRI were 75.9%, 77.5%, 74.5%, 72.1%, and 79.6%, respectively (Table 4).

Discussion

In the present study, we performed SWE ultrasonics to predict LN metastasis in patients with rectal cancer before individualized therapy and compared it with MRI.

LN metastasis is one of the key indications for preoperative neoadjuvant chemotherapy and also an important prognostic factor for local recurrence (23). However, the lack of high sensitivity and specificity of imaging modalities for nodal staging might lead to many patients being over-treated or having delayed treatment with chemoradiotherapy. Previously, the widely accepted diagnostic criterion for malignant nodes was the size of the LN on MRI images (24). The size threshold for LN positivity has been a source of controversy in previous studies. Some studies used the size threshold of >5 mm to indicate positive LNs (25). While for others, a size threshold of >5 mm in short axis with heterogeneous signal or ill-defined margins were used as the diagnostic criteria for positive LNs (26). However, approximately 41.4% of LNs <5 mm are

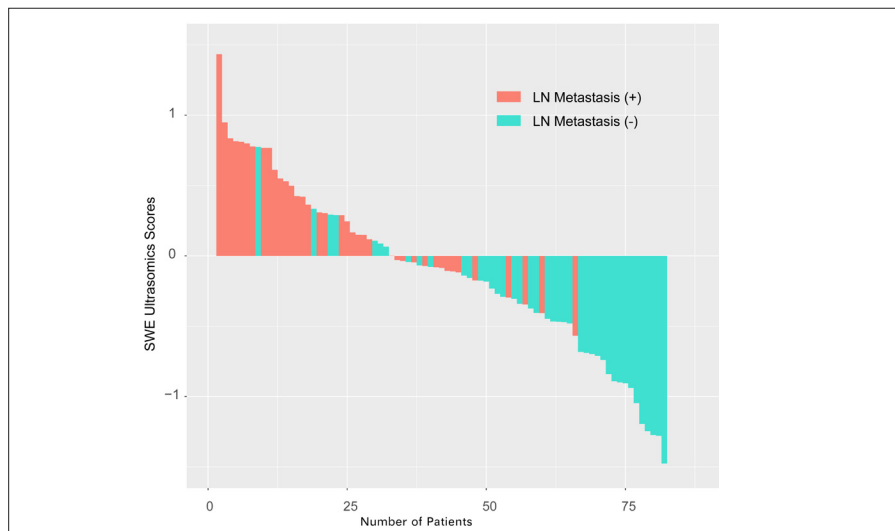


Figure 4. Diagram shows the SWE ultrasonics signature in 87 patients. Green bars represent negative LN involvement, and orange bars represent LN metastasis. The height of the bars represents the signature.

Table 4. The diagnostic performance of SWE ultrasonics and MRI

	AUC	Accuracy	95% CI	Sensitivity	Specificity	PPV	NPV
SWE ultrasonics	0.883	82.8%	0.732, 0.900	87.5%	78.8%	77.8%	88.1%
MRI	0.760	75.9%	0.655, 0.844	77.5%	74.5%	72.1%	79.6%

SWE, shear-wave elastography; MRI, magnetic resonance imaging; AUC, area under the ROC curve; 95% CI, 95% confidence interval; PPV, positive predictive value; NPV, negative predictive value.

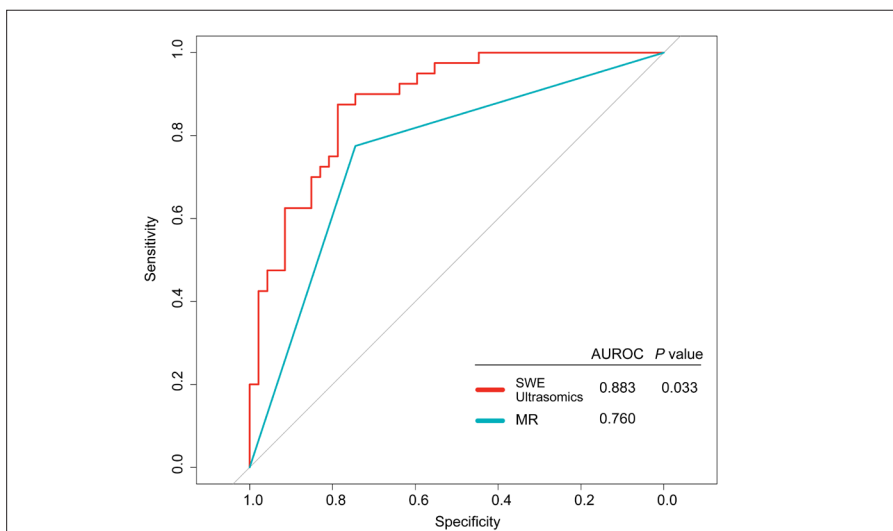


Figure 5. Predictive performance is assessed in terms of the area under receiver operator characteristic curve (AUC). Comparison of ROC curves between SWE ultrasonics and MRI in diagnosing LN metastasis of patients with rectal cancer. Red line represents SWE ultrasonics and blue line represents MRI.

positive for metastasis (27). Other imaging parameters in MRI, such as the border, shape or intrinsic signal of LNs, were analyzed in various studies, but the results have been inconsistent (19, 27, 28). Moreover, these features are subjective, due to a lack of objective quantitative indicators. Different physicians may have different opinions about the same LN, which may affect the accuracy of diagnosis.

Another important diagnostic tool for accurate evaluation of rectal tumors is EUS. In one report, the sensitivity and specificity of EUS in diagnosing nodal involvement were approximately 73.2% and 75.8%, respectively (12). In fact, the determination of LN involvement with EUS is less accurate because of the difficulty in discriminating between inflammatory and metastatic LNs, which leads to misdiagnosis and possible overtreatment. Moreover, the inspection scope of EUS is limited, which precludes full exploration of the pelvic cavity or iliac fossa LNs. These limitations weaken the usefulness of EUS for LN staging.

With the development of radiomics in recent years, these limitations may be

solved. Radiomics-based tools have been developed to improve diagnostic, prognostic, and predictive accuracy mainly in cancer disease. Wu et al. (29) developed an MRI-based radiomics signature of bladder tumor for the preoperative prediction of LN metastasis in patients. Similarly, Huang et al. (30) developed a radiomics model of primary tumor to predict LN status in colorectal cancer. Thus, the noninvasive radiomics signature of primary tumor, which makes use of the images we already obtained, could serve as a more convenient method for the prediction of LN metastasis. Recently, Chen et al. (31) developed a multiparametric ultrasonics nomogram to improve pre-therapeutic individualized prediction of LN metastasis. The nomogram incorporated EUS, CT and SWE features, with a C-index of 0.857–0.872. However, the study did not compare their diagnostic efficiency with other imaging methods, such as MRI.

In our study, ultrasonics features were extracted from the color map of the SWE containing the information of tissue stiffness. Red and darker images signify higher

stiffness of the lesions, while blue images represent soft tissue. Therefore, we believe that SWE ultrasonics data extracted from the color map of the SWE, which includes characteristics of lesion stiffness, distribution of stiffness, as well as the uniformity and heterogeneity of stiffness, may reflect the biological characteristics of the tumor more comprehensively, rather than the stiffness value measured by the SWE equipment.

Considering the above findings, we proposed a model of SWE-based ultrasonics for the preoperative prediction of LN metastasis in patients with rectal cancer. As indicated in our results, we found that the diagnostic performance of SWE ultrasonics for the detection of LN metastasis in patients with rectal cancer was significantly higher compared to that of MRI. Our results also demonstrated that among the 21 patients misdiagnosed by MRI, 17 patients were correctly identified by SWE ultrasonics. The high accuracy of SWE ultrasonics benefited from the application of numerous quantitative ultrasonics parameters rather than the use of subjective evaluation (e.g., signal, boundary). Therefore, the overall diagnostic efficiency of SWE ultrasonics was higher than that of MRI.

In this study, the selected 13 high-throughput ultrasonics parameters, including histogram parameters, texture parameters, GLCM parameters and GLRLM parameters, are crucial for the evaluation of LN metastasis in rectal cancer. These parameters may fully reflect the biological characteristics of tumors. For example, histogram parameters have been applied to describe the distribution of voxel intensities of the lesion. Textural features calculated from GLCM and GLRLM can quantify intratumor heterogeneity.

Our study limitations included the relatively small sample size; thus, a future multicenter study with a larger sample size is mandatory. In addition, no subgroup analysis, such as the SWE ultrasonics difference between T1/2 and T3/4 tumors, was performed. Finally, EUS is an endoluminal

examination. Considering the tolerance and compliance of patients, we did not perform intra- and inter-radiologist reliability on multiple examinations. Beyond that, the comparison between SWE-based ultrasomics and MRI radiomics was not performed in our study. It has been reported that the preoperative radiomic signature based on multiparametric MRI has been used for LN status prediction in rectal cancer (32). The MRI-based radiomics has AUC, accuracy, sensitivity, and specificity of 0.677, 0.610, 0.762, and 0.494, respectively. Therefore, the comparison between SWE based ultrasomics and MRI radiomics will be performed in an upcoming study.

In conclusion, this study demonstrated that SWE ultrasomics is a more accurate predictive tool than MRI for identifying LN metastasis preoperatively. Thus, SWE ultrasomics might be conveniently used to guide preoperative individualized therapies for patients with rectal cancer.

Financial disclosure

This work was supported by the National Nature Science Foundation of China [grant numbers 81701719, 81701701, 81601500]; Guangdong Finance Foundation [grant number 20160904]; and Training Project for Young Teacher of Sun Yat-sen University [grant number 16YKPY37].

Conflict of interest disclosure

The authors declared no conflicts of interest.

References

- Brenner H, Kloor M, Pox CP. Colorectal cancer. *Lancet* 2014; 383:1490–1502. [\[Crossref\]](#)
- Benson AB, 3rd, Venook AP, Al-Hawary MM, et al. Rectal Cancer, version 2.2018, NCCN clinical practice guidelines in oncology. *J Natl Compr Canc Netw* 2018; 16:874–901. [\[Crossref\]](#)
- Smith N, Brown G. Preoperative staging of rectal cancer. *Acta Oncol* 2008; 47:20–31. [\[Crossref\]](#)
- Chang GJ, Rodriguez-Bigas MA, Skibber JM, Moyer VA. Lymph node evaluation and survival after curative resection of colon cancer: Systematic review. *J Natl Cancer Inst* 2007; 99:433–441. [\[Crossref\]](#)
- Tudyka V, Blomqvist L, Beets-Tan RG, et al. EURECCA consensus conference highlights about colon & rectal cancer multidisciplinary management: The radiology experts review. *Eur J Surg Oncol* 2014; 40:469–475. [\[Crossref\]](#)
- Engstrom PF, Arnoletti JP, Benson AB, 3rd, et al. NCCN clinical practice guidelines in oncology: Rectal cancer. *J Natl Compr Canc Netw* 2009; 7:838–881. [\[Crossref\]](#)
- Mortenson MM, Khatri VP, Bennett JJ, Petrelli NJ. Total mesorectal excision and pelvic node dissection for rectal cancer: An appraisal. *Surg Oncol Clin North Am* 2007; 16:177–197. [\[Crossref\]](#)
- Moreno CC, Sullivan PS, Mittal PK. MRI evaluation of rectal cancer: Staging and restaging. *Curr Probl Diagn Radiol* 2017; 46:234–241. [\[Crossref\]](#)
- Al-Sukhni E, Milot L, Fruitman M, et al. Diagnostic accuracy of MRI for assessment of T category, lymph node metastases, and circumferential resection margin involvement in patients with rectal cancer: A systematic review and meta-analysis. *Ann Surg Oncol* 2012; 19:2212–2223. [\[Crossref\]](#)
- Cartana ET, Parvu D, Saftoiu A. Endoscopic ultrasound: Current role and future perspectives in managing rectal cancer patients. *J Gastrointest Liver Dis* 2011; 20:407–413.
- Cosgrove D, Piscaglia F, Bamber J, et al. EfsUMB guidelines and recommendations on the clinical use of ultrasound elastography. Part 2: Clinical applications. *Ultraschall Med* 2013; 34:238–253. [\[Crossref\]](#)
- Puli SR, Reddy JB, Bechtold ML, Choudhary A, Antillon MR, Brugge WR. Accuracy of endoscopic ultrasound to diagnose nodal invasion by rectal cancers: A meta-analysis and systematic review. *Ann Surg Oncol* 2009; 16:1255–1265. [\[Crossref\]](#)
- Herzog U, von Flue M, Tondelli P, Schuppisser JP. How accurate is endorectal ultrasound in the preoperative staging of rectal cancer? *Dis Colon Rectum* 1993; 36:127–134. [\[Crossref\]](#)
- Kumar V, Gu Y, Basu S, et al. Radiomics: The process and the challenges. *Magn Reson Imaging* 2012; 30:1234–1248. [\[Crossref\]](#)
- Lambin P, Leijenaar RTH, Deist TM, et al. Radiomics: The bridge between medical imaging and personalized medicine. *Nat Rev Clin Oncol* 2017; 14:749–762. [\[Crossref\]](#)
- Li W, Huang Y, Zhuang BW, et al. Multiparametric ultrasomics of significant liver fibrosis: A machine learning-based analysis. *Eur Radiol* 2018. [\[Crossref\]](#)
- Bamber J, Cosgrove D, Dietrich CF, et al. EfsUMB guidelines and recommendations on the clinical use of ultrasound elastography. Part 1: Basic principles and technology. *Ultraschall Med* 2013; 34:169–184. [\[Crossref\]](#)
- Wang K, Lu X, Zhou H, et al. Deep learning radiomics of shear wave elastography significantly improved diagnostic performance for assessing liver fibrosis in chronic hepatitis B: A prospective multicentre study. *Gut* 2019; 68:729–741. [\[Crossref\]](#)
- Brown G, Richards CJ, Bourne MW, et al. Morphologic predictors of lymph node status in rectal cancer with use of high-spatial-resolution MR imaging with histopathologic comparison. *Radiology* 2003; 227:371–377. [\[Crossref\]](#)
- Liu L, Liu M, Yang Z, He W, Wang Z, Jin E. Correlation of MRI-detected extramural vascular invasion with regional lymph node metastasis in rectal cancer. *Clin Imaging* 2016; 40:456–460. [\[Crossref\]](#)
- Tang Y, Rao S, Yang C, Hu Y, Sheng R, Zeng M. Value of MRI morphologic features with pt1-2 rectal cancer in determining lymph node metastasis. *J Surg Oncol* 2018; 118:544–550. [\[Crossref\]](#)
- Edge SB, Compton CC. The American joint committee on cancer: The 7th edition of the ajcc cancer staging manual and the future of tmn. *Ann Surg Oncol* 2010; 17:1471–1474. [\[Crossref\]](#)
- Hermanek P, Merkel S, Fietkau R, Rodel C, Hohenberger W. Regional lymph node metastasis and locoregional recurrence of rectal carcinoma in the era of tme [corrected] surgery. Implications for treatment decisions. *Int J Colorectal Dis* 2010; 25:359–368. [\[Crossref\]](#)
- Ogawa S, Itabashi M, Hirotsawa T, Hashimoto T, Bamba Y, Kameoka S. Lateral pelvic lymph node dissection can be omitted in lower rectal cancer in which the longest lateral pelvic and perirectal lymph node is less than 5 mm on MRI. *J Surg Oncol* 2014; 109:227–233. [\[Crossref\]](#)
- Iannicelli E, Di Renzo S, Ferri M, et al. Accuracy of high-resolution MRI with lumen distention in rectal cancer staging and circumferential margin involvement prediction. *Korean J Radiol* 2014; 15. [\[Crossref\]](#)
- Park JS JY-J, Choi G-S, et al. Accuracy of preoperative MRI in predicting pathology stage in rectal cancers: Node-for-node matched histopathology validation of MRI features. *Dis Colon Rectum* 2014; 57:32–38. [\[Crossref\]](#)
- Liu Y, Wang R, Ding Y, et al. A predictive nomogram improved diagnostic accuracy and interobserver agreement of perirectal lymph nodes metastases in rectal cancer. *Oncotarget* 2016; 7:14755–14764. [\[Crossref\]](#)
- Klessen C, Rogalla P, Taupitz M. Local staging of rectal cancer: The current role of MRI. *Eur Radiol* 2007; 17:379–389. [\[Crossref\]](#)
- Wu S, Zheng J, Li Y, et al. Development and validation of an MRI-based radiomics signature for the preoperative prediction of lymph node metastasis in bladder cancer. *EBioMedicine* 2018; 34:76–84. [\[Crossref\]](#)
- Huang Y-q, Liang C-h, He L, et al. Development and validation of a radiomics nomogram for preoperative prediction of lymph node metastasis in colorectal cancer. *J Clin Oncol* 2016; 34:2157–2164. [\[Crossref\]](#)
- Chen LD, Liang JY, Wu H, et al. Multiparametric radiomics improve prediction of lymph node metastasis of rectal cancer compared with conventional radiomics. *Life Sci* 2018; 208:55–63. [\[Crossref\]](#)
- Meng X, Xia W, Xie P, et al. Preoperative radiomic signature based on multiparametric magnetic resonance imaging for noninvasive evaluation of biological characteristics in rectal cancer. *Eur Radiol* 2019; 29:3200–3209. [\[Crossref\]](#)